Transactions on Machine Intelligence 4(3) (2021) 169-181

ISSN Online: 2821-1693

Transactions on Machine Intelligence

Journal Homepage: https://tmachineintelligence.ir/index.php/TMI

Enhancement of the Ring-Shaped Photonic Crystal Raman Amplifier Using Optofluidic Materials

A. Seyedfaraji [1,*]

[1] Associate Professor, Department of Electrical Engineering, Faculty of Engineering, Alzahra University, Tehran, Iran

ARTICLE INFO

Article History:
Received 7 April 2021
Received in revised form 26 May 2021
Accepted 27 September 2021
Available online 28 September 2021

Keywords:
Raman Amplifier, Ring Structure, Photonic Crystal, Optofluidic Materials, Bit Rate, Maxwell's Equations.

ABSTRACT

This study explores the potential of a ring-shaped photonic crystal structure for Raman amplification, focusing on the integration of optofluidic materials to enhance performance. By incorporating optofluidic cavities on both sides of the signal transmission path, the effective refractive index of the medium is modified, leading to a reduction in the group velocity of both the pump and signal waves. This reduction enhances the interaction time between the optical waves, thereby increasing the Raman gain. To further improve performance, a dual-ring structure is introduced and analyzed, comparing its efficiency with that of a single-ring configuration. The impact of structural modifications on the achievable bit rate is also investigated. The numerical analysis is conducted using the Finite-Difference Time-Domain (FDTD) method, solving Maxwell's equations while accounting for various nonlinear effects, including two-photon absorption (TPA), free-carrier absorption (FCA), the Kerr effect, and self-phase modulation (SPM) in a hybrid photonic crystal waveguide. The proposed design, with a compact length of only 100 μm, demonstrates a significant Raman gain of 19.01 dB. Additionally, the system achieves an impressive bit rate of 0.6493×10^{12} pulses per second, making it a promising candidate for high-speed, high-gain optical signal amplification in next-generation photonic communication networks.

1. INTRODUCTION

Silicon (Si) plays a crucial role in the development of amplifiers, optical sources, high-speed modulators, and photodetectors. Silicon-based photonics has been widely utilized in various fields, including medical applications, military technologies, and optical communications. In recent years, Raman amplification and light generation in silicon via stimulated Raman scattering have attracted significant attention [1].

In spontaneous Raman scattering, thermal lattice vibrations at frequency ωυ induce a sinusoidal modulation in the optical susceptibility. In silicon, this frequency is approximately 15.6 THz. When the oscillations of the incident pump field at frequency ωl interact with the optical susceptibility oscillations at frequency ωυ, polarizations at the sum frequency (ωl+ωυ) and difference frequency (ωl-ωυ) are generated. The radiation corresponding to these polarization components is referred to as anti-Stokes and Stokes waves, respectively. In stimulated Raman scattering,

* Corresponding Author: sfaraji@alzahra.ac.ir
Associate Professor, Department of Electrical Engineering, Faculty of Engineering, Alzahra University, Tehran, Iran

http://dx.doi.org/10.47176/TMI.2021.169

atomic vibrations can be excited coherently by simultaneously propagating the pump and Stokes fields with a frequency difference equal to the atomic vibration frequency in the Raman medium, thereby amplifying the Stokes field [2].

In recent years, Raman gain in silicon waveguides has been extensively studied [3–5]. To enhance the performance of Raman amplifiers, various approaches have been explored, including silicon nano waveguides [6], SiGe waveguides [7], photonic crystal waveguides [8,9], hybrid photonic crystals [10], and slow-light photonic crystal waveguides [11]. Design principles for Raman amplifiers have been formulated using analytical and semi-analytical methods [12], and waveguide geometries have been optimized to achieve higher Raman gain and improved amplification efficiency [13].

Moreover, reducing the speed of light propagation within a medium increases the interaction time between light and matter, thereby enhancing nonlinear effects. Operating in the slow-light regime reduces the required pump power and physical length necessary for the onset of nonlinear effects. Consequently, slow-light structures are employed to minimize the dimensions of optical devices and enhance nonlinear interactions [14,15].

In photonic crystal waveguides, Bragg reflections enhance the optical confinement factor and reduce the group velocity. A high optical confinement factor minimizes pump power loss, while a lower group velocity increases the interaction time between light and matter. These factors intensify nonlinear effects such as Raman scattering, enabling higher Raman gain at lower pump power levels. Analytical studies have also demonstrated that reducing the group velocity in photonic crystal waveguides results in enhanced Raman gain [16].

To optimize pump power utilization, we previously introduced novel ring-shaped Raman amplifiers [17] and ring Raman amplifiers integrated within photonic crystal and hybrid photonic crystal platforms [18]. In ring structures, pump resonance enhances the pump power within the micro ring, allowing for greater Raman gain at lower input pump power compared to conventional straight waveguides.

In this study, we investigate a ring-shaped photonic crystal Raman amplifier and analyze the impact of incorporating optofluidic materials [19,20] to reduce the group velocity and enhance Raman gain. The photonic crystal structure, along with the use of optofluidic materials, increases dispersion along the amplifier, which in turn reduces the data transmission bit rate. The transmission bit rate in the proposed structures will also be evaluated in this work.

The structure of this paper is as follows: Section 2 presents the modeling of Raman amplification in hybrid photonic crystal waveguides based on Maxwell's equations, incorporating nonlinear effects such as two-photon absorption (TPA), free-carrier absorption (FCA), the Kerr effect, and self-phase modulation (SPM). Section 3 discusses the simulation results of Raman amplification in ring-shaped photonic crystals and their enhanced versions incorporating optofluidic materials. Finally, Section 4 provides a conclusion summarizing the findings of this study.

2. THEORETICAL MODELING

The refractive index of the waveguide depends on the power of the propagating light, as nonlinear effects such as two-photon absorption, the Kerr effect, and other nonlinear phenomena alter the refractive index based on the intensity of the transmitted light [21]. When a high-intensity optical pulse propagates through the medium, nonlinear effects induce a phase shift of magnitude $\Delta\varphi$.

If the pump is continuous, the intensity and phase variation remain constant over time. However, when short, high-intensity pump pulses are used, the pump intensity changes rapidly with time, leading to rapid temporal variations in phase. The time derivative of the phase variation results in a frequency chirp $\Delta\omega$ [21].

$$\Delta\omega(x,y,t) = -\frac{d(\Delta\varphi(x,y,t))}{dt} \tag{1}$$

where $\varphi\Delta$ is obtained from equation (2) [21].

$$\Delta\varphi(x,y,t) = \frac{2\pi L_{int}}{\lambda_{P_{kerr_{FC}}}} \tag{2}$$

L_{int} represents the interaction length of light and the medium, Δn_{kerr} denotes the refractive index change due to the Kerr effect, Δn_{FC} represents the refractive index change caused by free carriers, and λ_P is the central wavelength of the pulsed pump within the waveguide. Δω are induced. Furthermore, as the pulse passes through each point, the carrier density increases, leading to an elevation in the refractive index. Consequently, the central wavelength will experience a blue shift. The central wavelength at each point is derived from Equation (3) [21].

$$\lambda_P(x,y,t) = \frac{\lambda_0}{1 - (\frac{L_{int}}{c}\frac{d\Delta n(x,y,t)}{dt}} \tag{۳}$$

In this context, Δn represents the sum of the refractive index variations induced by the nonlinear Kerr effect and free-carrier absorption (FCA). Here λ_0 denotes the initial wavelength of the input pump, and ccc is the speed of light. As the pump power increases, losses due to two-photon absorption (TPA) and free-carrier absorption (FCA) become more significant. Therefore, accounting for these phenomena in simulations is essential [22]. Raman scattering and two-photon absorption (TPA) are modeled using the third-order nonlinear optical susceptibility [23, 24]. The TPA effect alters the carrier density, which in turn affects both the refractive index and the gain coefficient. Consequently, both the real and imaginary components of the first-order optical susceptibility are influenced [24]. The self-phase modulation (SPM) effect is modeled by the real part of the third-order nonlinear optical susceptibility. Considering these effects, the electric polarization vector for the pump and signal fields is expressed by Equations (4) and (5).

$$\mathbf{P_S} = \mathbf{P}(\omega_S) = \chi(\omega_S)\mathbf{E_S} + \varepsilon_0\chi^{(3)}_{\mathrm{Im}}(\omega_S)\mathbf{E_P}.\mathbf{E_P^*}.\mathbf{E_S} + \varepsilon_0\chi^{(3)}_{\mathrm{Im}}(\omega_S)\mathbf{E_S}.\mathbf{E_S^*}.\mathbf{E_S} + \varepsilon_0\chi_P^{(f)}(\omega_S,N)\mathbf{E_S} \tag{4}$$

$$\begin{aligned}\mathbf{P_P} = \mathbf{P}(\omega_P) = {} & \chi(\omega_P)\mathbf{E_P} + \varepsilon_0\chi^{(3)}_{\mathrm{Im}}(\omega_P)\mathbf{E_S}.\mathbf{E_S^*}.\mathbf{E_P} + \varepsilon_0\chi^{(3)}_{\mathrm{Im}}(\omega_P)\mathbf{E_P}.\mathbf{E_P^*}.\mathbf{E_P} \\ & + \varepsilon_0\chi_P^{(f)}(\omega_P,N)\mathbf{E_P} + \varepsilon_0\chi^{(3)}_{\mathrm{Re}}(\omega_P)\mathbf{E_P}.\mathbf{E_P^*}.\mathbf{E_P}\end{aligned} \tag{5}$$

In these equations, $\mathbf{E_S}$ represents the electric field of the signal, $\mathbf{E_P}$ denotes the electric field of the pump, NN is the carrier density, and ω_S and ω_P correspond to the signal and pump frequencies, respectively. χ is the first-order optical susceptibility, while $\chi^{(3)}_{Im}$ and $\chi^{(3)}_{Re}$ represent the imaginary and real parts of the third-order optical susceptibility, respectively. $\chi^{(f)}$, which models the FCA effect, is defined as follows [24].

$$\chi_v^{(f)} = 2n_0\left(n_{fv} + ic\frac{\alpha_{fv}}{2\omega_v}\right) \tag{6}$$

$$n_{fv}(\omega_v,N) = -\frac{q^2N}{2\varepsilon_0 n_0\omega_v^2}\left(\frac{1}{m_{ce}} + \frac{1}{m_{ch}}\right) \tag{7}$$

$$\alpha_{fv}(\omega_v,N) = \frac{q^3N}{\varepsilon_0 cn_0\omega_v^2}\left(\frac{1}{\mu_e m_{ce}^2} + \frac{1}{\mu_h m_{ch}^2}\right) \tag{8}$$

In these relations, *v* is substituted for *S* to denote the signal and *P* for the pump. n_0 represents the linear refractive index, n_{fv} denotes the changes in the refractive index due to variations in carrier density, and α_{fv} represents the changes in the absorption coefficient due to variations in carrier density. m_{ce} ، m_{ch} ، μ_e and μ_h are the effective mass of the electron, the effective mass of the hole, the electron mobility, and the hole mobility, respectively [24]. The variations in carrier density are described by equations (9), (10), and (11).

$$\frac{dN}{dt} = -\frac{N}{\tau} + \frac{\beta_2(\omega_S)I_S^2}{2\hbar\omega_S} + \frac{\beta_2(\omega_P)I_P^2}{2\hbar\omega_P} \tag{9}$$

$$I_S = \frac{\varepsilon_0 cn}{2}\left|\mathrm{E}_S\right|^2 \qquad I_P = \frac{\varepsilon_0 cn}{2}\left|\mathrm{E}_P\right|^2 \tag{10}$$

$$\beta_2(\omega) = \frac{3\omega\chi_{Im}^{(3)}}{2\varepsilon_0 c^2 n_0^2} \tag{11}$$

Where β_2 is the TPA coefficient, τ represents the carrier lifetime, and n_0 denotes the initial refractive index of the waveguide.

The Kerr effect links the linear refractive index of the material to the power of the propagating optical field. This relationship is expressed by Equation (12) [21].

$$n = n_0 + n_2 I_P \tag{12}$$

Where n_2 is referred to as the Kerr coefficient.

By considering nonlinear effects and utilizing the equations for electric polarization, the relative permittivity at each point can be determined and substituted into Maxwell's equations. These equations are then solved using the finite-difference time-domain (FDTD) method with perfectly matched layer (PML) boundary conditions.

3. DISCUSSION AND ANALYSIS OF SIMULATION RESULTS

Figure 1(a) illustrates the ring-shaped Raman amplifier with a photonic crystal structure (SR), while Figure 1(b) presents the enhanced ring-shaped Raman amplifier incorporating optofluidic materials (SR_a).

In the hexagonal photonic crystal structure of Raman amplifiers, the periodicity is denoted as *a*, and the radius of the air holes is represented by *r*. In these configurations, the pump and signal inputs are separated. The pump enters the amplifier through the upper waveguide and is coupled into the ring via the coupling region. The coupling region and the perimeter of the ring are designed such that the pump resonance within the ring remains in the critical state, ensuring maximum amplification for the pump wavelength. Consequently, a high Raman gain is achieved even with a low input pump power. The signal is introduced into the amplifier through the lower waveguide.

Within this waveguide, air holes are positioned before and after the ring (denoted as sections **B** and **B'**). The radius and spacing of these air holes are designed to facilitate the low-loss transmission of the signal wavelength (TE, 1.686 μm), while preventing the passage of the pump wavelength (TM, 1.55 μm). These sections are referred to as pump filters, ensuring that the pump remains confined within the ring for further amplification.

Additionally, another set of air holes with specific spacing and radius is placed along two sides of the ring (denoted as sections **C** and **C'**). These structures prevent the signal from entering the ring, ensuring that it propagates only along the direct path of the lower waveguide and exits through the opposite end. These sections are designated as signal filters. The design of these air holes allows the pump to circulate within the ring with minimal loss. The geometric parameters of the SR and SR_a structures are provided in Table 1.

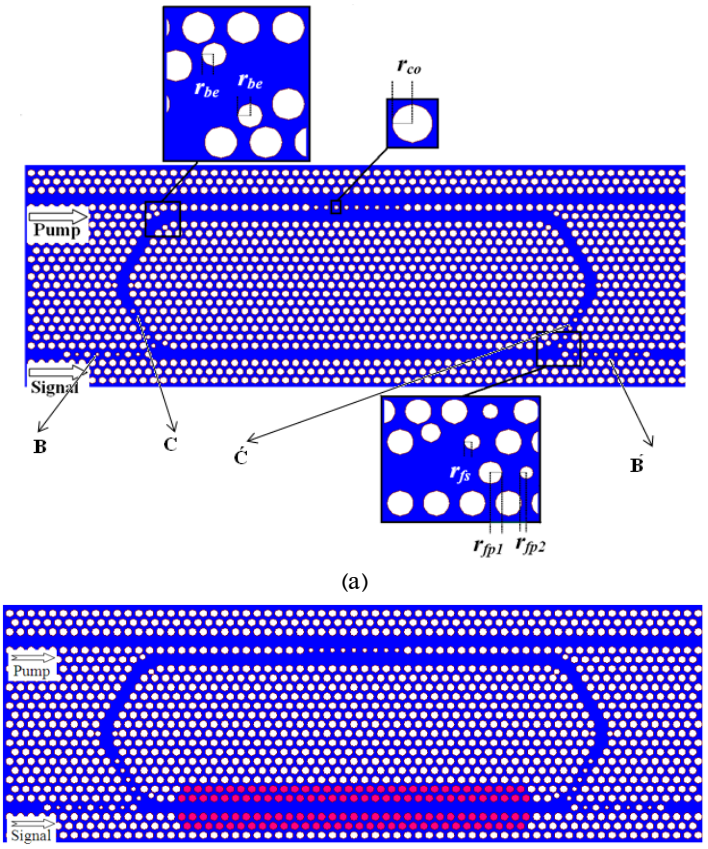

Fig. 1. Structure of ring-shaped Raman amplifiers: (a) Ring-shaped Raman amplifier with a photonic crystal structure (SR), and (b) Enhanced ring-shaped Raman amplifier with a photonic crystal structure incorporating optofluidic materials (SR_a).

Table 1. Physical Parameters of Ring-Shaped Raman Amplifiers

Parameter	SR	SR_a
a (nm)	460	**460**
r (nm)	165.6	**165.6**
r_{fs}(nm)	89.7	**89.7**
r_{fp1}(nm)	147.2	**147.2**
r_{fp2}(nm)	69	**69**
r_{co}(nm)	308.2	**308.2**
r_{be}(nm)	124.2	**124.2**
n_{of}	--	**1.5**

The transmission spectra of the pump filter and signal filter for the photonic crystal structures, around the pump and signal wavelengths, are shown in Figures 2 and 3, respectively.

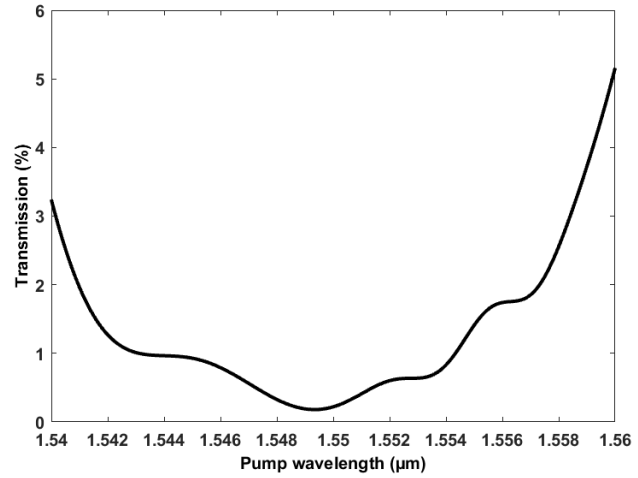

(a)

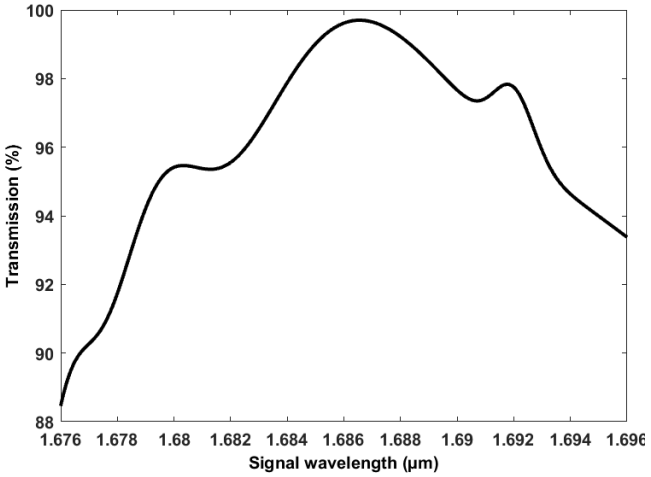

(b)

Fig. 2. Transmission spectra curves of the pump filter around (a) the pump wavelength and (b) the signal wavelength for photonic crystal structures.

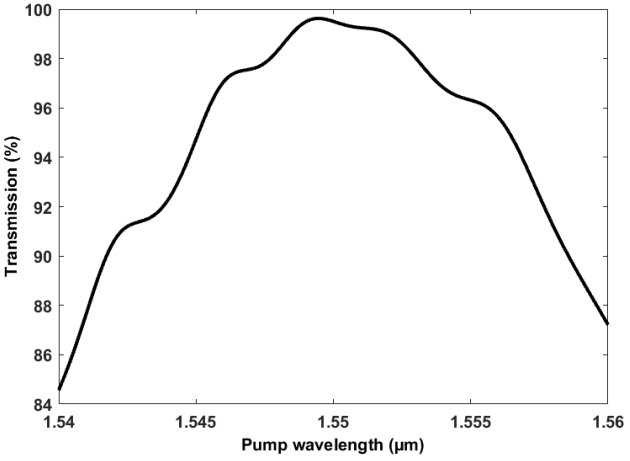

(a)

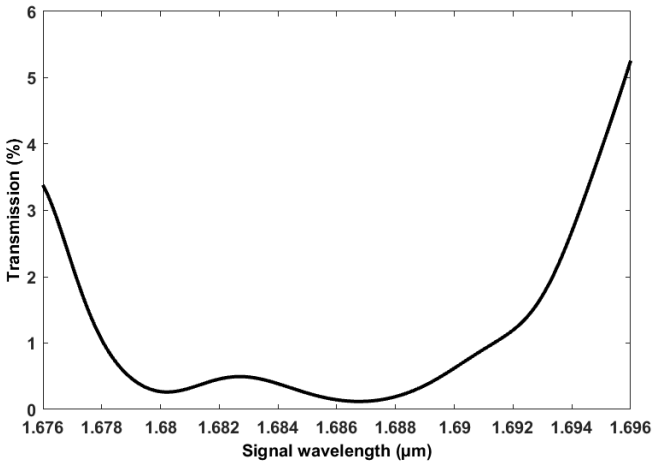

(b)

Fig. 3. Transmission spectra curves of the signal filter around (a) the pump wavelength and (b) the signal wavelength for photonic crystal structures.

Another important aspect is the design of the bending regions in the photonic crystal structures. Various methods exist to improve the transmission quality in these bending regions [26, 25, 20, 19]. In this work, based on [25], the bending regions are designed such that the radius of the air hole at the inner corner of the bend is reduced (r_{be}= 0.75 × r) while at the outer corner of the bend, an air hole with a radius of (r_{be}) is created. Both small holes are displaced by 0.3×a along the symmetry axis of the bend, in opposite directions. The transmission spectra curves for the bending regions in the photonic crystal are shown in Figure 4. The pump wavelength passes through the bending region with minimal loss.

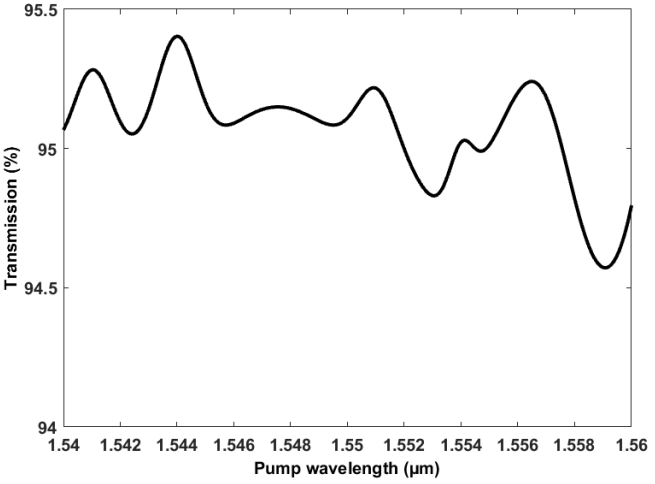

Fig. 4. Transmission spectra curve of the bending regions around the pump wavelength for the photonic crystal structure.

In the structure shown in Figure 1(b), two rows of holes on both sides of the signal propagation path are filled with optofluidic materials with a refractive index (n_{of}).

Figure 5 shows the Raman gain along the amplification region for the two introduced structures and for a pump power of 0.3W. At the beginning and end of each curve, there is a region where no amplification occurs, corresponding to the signal passing through the pump filter.

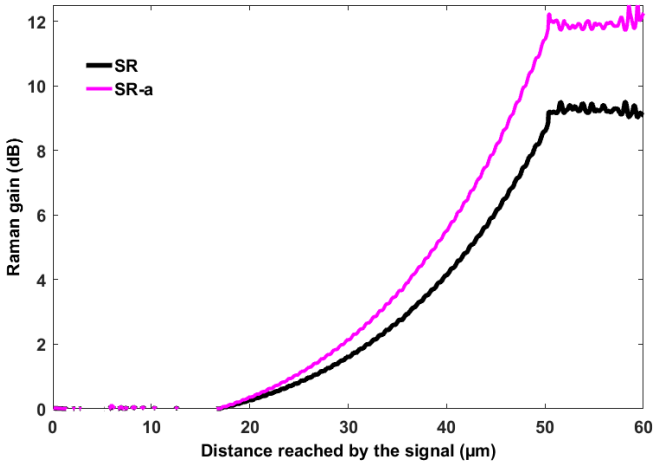

Fig. 5. Raman gains along the amplification region for the two structures, SR and SR-a. The input pump power is 0.3W.

The presence of optofluidic materials on both sides of the signal propagation path reduces the group velocity of the pump and signal in this path. The reduction in group velocity increases the interaction time between the pump and signal, resulting in a larger Raman gain. For the signal path length of approximately 60 μm, the Raman gain in the SR_a structure is approximately 3 dB larger than the Raman gain achieved from the SR structure.

To achieve a larger Raman gain with a fixed input pump power, two rings can be placed along each other as shown in Figure 6, ensuring that the rings do not couple with each other and are placed at the minimum distance from one another.

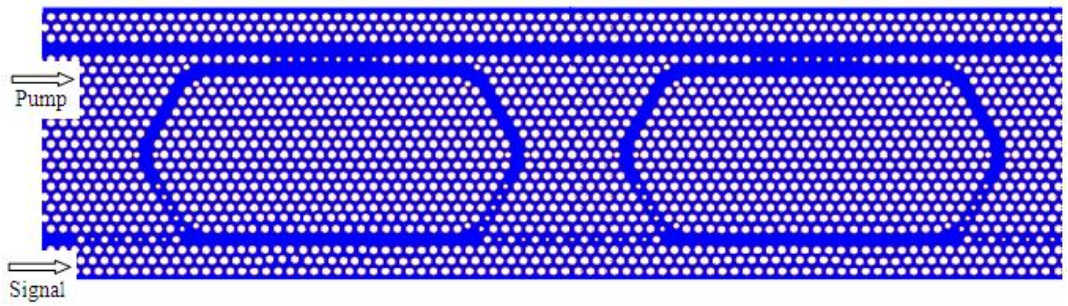

Fig. 6. Two-ring photonic crystal Raman amplifier structure.

Figure 7 shows the Raman gain along the amplification region for the two-ring SR and SR-a structures with an input pump power of 0.3W. According to this graph, for a fixed input pump power, the Raman gain in the two-ring structure is nearly twice that of the single-ring structure. The amplification from the second ring is slightly lower than that of the first ring, which is due to the lower pump intensity in the second ring. The regions where no amplification occurs correspond to the signal passing through the pump filter.

Another point is that the use of optofluidic materials in the improved photonic crystal structure results in a Raman gain increase of approximately 6 dB along a length of about 100 μm compared to the photonic crystal structure.

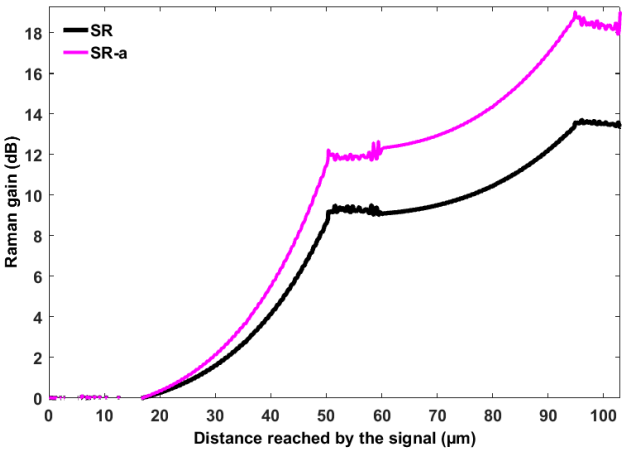

Fig. 7. Raman gain along the amplification region for the two-ring SR and SR-a structures. The input pump power is 0.3W.

Figure 8 and Figure 9 show three consecutive signal pulses at the output of the Raman amplifiers for the single-ring and two-ring structures, respectively. The propagation of the signal pulse inside the waveguide causes dispersion, leading to pulse broadening in the time domain and a decrease in the amplifier's bit rate. The use of a two-ring structure increases dispersion and further reduces the bit rate. The input pump power of 0.3W is considered. The Raman gains and dispersion in the SR-a amplifier are higher than in the SR amplifier. The use of optofluidic materials in the SR-a structure results in a significant increase in Raman gain, but slightly increases dispersion. Therefore, the SR-a structure provides a high gain while maintaining a reasonable bit rate.

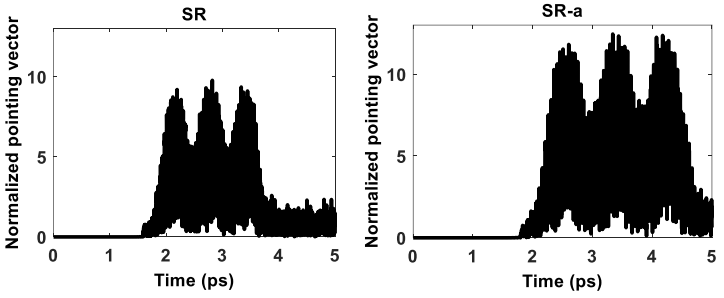

Fig. 8. Three consecutive signal pulses at the output of single-ring Raman amplifiers SR and SR-a. The input pump power is 0.3 W.

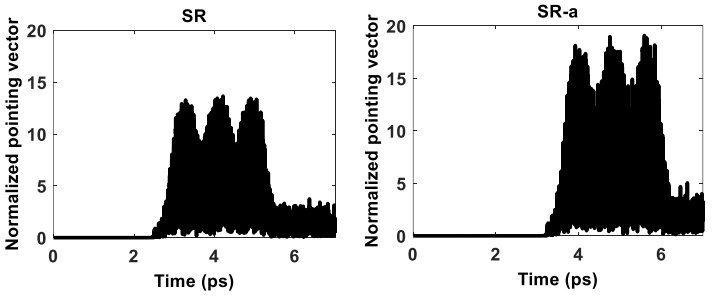

Fig. 9. Three consecutive signal pulses at the output of dual-ring Raman amplifiers SR and SR-a. The input pump power is 0.3 W.

Additionally, you mentioned the Fourier transform of the output signal pulses shown in Figure 10, which highlights the dispersion effect in the time domain. The dispersion leads to a reduction in the Full Width at Half Maximum (FWHM) in the frequency domain.

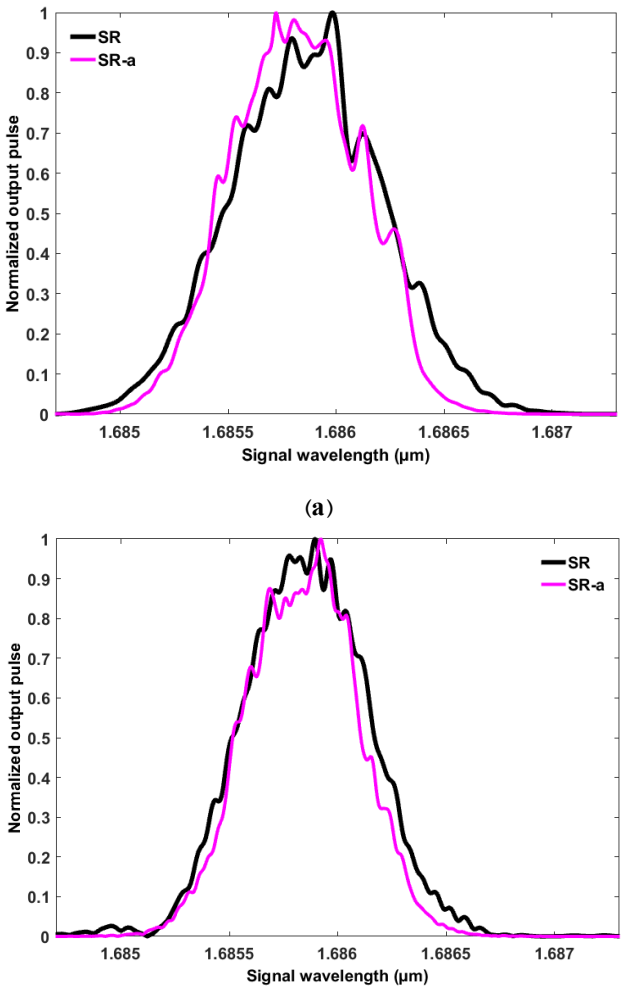

Fig. 10. Fourier transform of the output signal pulse in ring Raman amplifiers SR and SR-a. (a) Single-ring, (b) Dual-ring. The input pump power is 0.3 W.

The comparison between the SR and SR-a structures, in terms of Raman gain, bit rate, and the Full Width at Half Maximum (FWHM) of the Fourier transform of the output pulses, is summarized in Table 2. This comparison helps evaluate the performance of the two configurations.

4. CONCLUSION

In this paper, the ring photonic crystal (SR) and the enhanced photonic crystal (SR-a) structures for Raman amplification were compared. The use of optofluidic materials in the cavities on both sides of the signal path in the enhanced photonic crystal structure resulted in a significant increase in Raman gain. In the single-ring structure, Raman gain increased from 9.192 dB to 12.19 dB. The increase in Raman gain was even higher in the two-ring structure. The Raman gain in the two-ring photonic crystal structure was 13.56 dB. The use of optofluidic materials in the two-ring structure increased the Raman gain to 19.10 dB.

On the other hand, the propagation of signal pulses inside the waveguide causes dispersion, which in turn leads to pulse broadening in the time domain and a reduction in the amplifier's bit rate. The dispersion increases with the use of optofluidic materials or the two-ring structure. Therefore, the data transmission rate will decrease. However, according to Table 2, the decrease in the bit rate is not significant and can be considered less important compared to the increase in Raman gain. Thus, for signal amplification, the use of a two-ring photonic crystal amplifier enhanced by optofluidic materials is recommended.

Table 2. Raman Gain, Bit Rate, and FWHM of the Output Pulse Fourier Transform for Single-Ring Raman Amplifier Structures with an Input Pump Power of W 3/0

	SR (single-ring)	SR-a (single-ring)	SR (2-ring)	SR-a (2-ring)
Raman Gain (dB)	9.192	12.19	13.56	19.01
Bit Rate ($\times 10^{12}$ sec)	0.759	0.716	0.7077	0.6493
FWHM (nm)	0.79	0.77	0.69	0.64

This table summarizes the key performance parameters of the different structures, comparing the Raman gain, bit rate, and the Full Width at Half Maximum (FWHM) of the output pulse in each configuration.

Transparency Statement

The data supporting this study are available upon reasonable request to the corresponding author, subject to ethical and confidentiality considerations.

Acknowledgments

We would like to express our gratitude to all individuals who contributed to this project.

Declaration of Interest

The authors declare that they have no competing interests.

Funding

This research received no specific grant from any funding agency, commercial, or not-for-profit sectors.

REFERENCES

[1] Rong, H., Xu, S., Kuo, Y. H., Sih, V., Cohen, O., Raday, O., & Paniccia, M. (2007). Monolithic integrated ring resonator Raman silicon laser and amplifier. Proc. SPIE, 6485, 1-8. https://doi.org/10.1117/12.714210

[2] Jalali, B., Raghunathan, V., & Shori, R. (2006). Prospects of silicon Mid-IR Raman lasers. IEEE Journal of Selected Topics in Quantum Electronics, 12, 1618-1627. https://doi.org/10.1109/JSTQE.2006.885340

[3] Claps, R., Raghunathan, V., Dimitropoulos, D., & Jalali, B. (2004). Influence of nonlinear absorption on Raman amplification in silicon waveguides. Optics Express, 12, 2774-2780. https://doi.org/10.1364/OPEX.12.002774

[4] Liu, A., Rong, H., & Paniccia, M. (2004). Net optical gain in a low loss silicon-on-insulator waveguide by stimulated Raman scattering. Optics Express, 12, 4261-4268. https://doi.org/10.1364/OPEX.12.004261

[5] Rukhlenko, I. D., & Premaratne, M. (2010). Spectral compression and group delay of optical pulses in silicon Raman amplifiers. Opt. Lett., 35, 3138-3140. https://doi.org/10.1364/OL.35.003138

[6] Kroeger, F., Ryasnyanskiy, A., Baron, A., Dubreuil, N., Delaye, P., Frey, R., Roosen, G., & Peyrade, D. (2010). Saturation of the Raman amplification by self-phase modulation in silicon nanowaveguides. Applied Physics Letters, 96, 241102-1-241102-3. https://doi.org/10.1063/1.3451466

[7] Claps, R., Raghunathan, V., Boyraz, O., Koonath, P., Dimitropoulos, D., & Jalali, B. (2005). Raman amplification and lasing in SiGe waveguides. Optics Express, 13, 2459-2466. https://doi.org/10.1364/OPEX.13.002459

[8] Seidfaraji, A., & Ahmadi, V. (2012). Enhanced Raman amplification by photonic crystal based waveguide structure. ICTON, 1-4. https://doi.org/10.1109/ICTON.2012.6254408

[9] Seyedfaraji, A., & Ahmadi, V. (2013). Improvement of Raman amplifier bandwidth by means of slow light in photonic crystal based waveguide structure. Optical and Quantum Electronics, 45, 1237-1248. https://doi.org/10.1007/s11082-013-9744-7

[10] Seyedfaraji, A., & Ahmadi, V. (2010). Enhanced Raman amplification by hybrid photonic crystals. ICTON, 1-4. https://doi.org/10.1109/ICTON.2010.5549046

[11] Yi-Hua, H., Iwamoto, S., & Arakawa, Y. (2013). Design of slow-light grating waveguides for silicon Raman amplifier. CLEO-PR, 1-2. https://doi.org/10.1109/CLEOPR.2013.6600134

[12] Krause, M., Renner, H., & Brinkmeyer, E. (2010). Silicon Raman amplifiers with ring-resonator-enhanced pump power. IEEE J. Sel. Top. Quant., 16, 216-225. https://doi.org/10.1109/JSTQE.2009.2025607

[13] Rukhlenko, I. D., Dissanayake, C., Premaratne, M., & Agrawal, G. P. (2010). Optimization of Raman amplification in silicon waveguide with finite facet reflectivities. IEEE J. Sel. Top. Quant., 16, 226-233. https://doi.org/10.1109/JSTQE.2009.2030512

[14] Monat, C., Corcoran, B., Pudo, D., Ebnali-Heidari, M., Grillet, C., Pelusi, M. D., Moss, B. J., Eggleton, D. J., White, T. P., O'Faolain, L., & Krauss, T. F. (2010). Slow light enhanced nonlinear optics in silicon photonic crystal waveguides. IEEE J. Sel. Top. Quantum Electron., 16, 344-356. https://doi.org/10.1109/JSTQE.2009.2033019

[15] Corcoran, B., Monat, C. D., Pelusi, M., Grillet, C., White, T. P., O'Faolain, L., Krauss, T. F., Eggleton, B. J., & Moss, D. J. (2010). Optical signal processing on a silicon chip at 640Gb/s using slow-light. Opt. Express, 18, 7770-7781. https://doi.org/10.1364/OE.18.007770

[16] McMillan, J. F., Yang, X., Panoiu, N. C., Osgood, R. M., & Wong, C. W. (2006). Enhanced stimulated Raman scattering in slow-light photonic crystal waveguides. Optics Letters, 31, 1235-1237. https://doi.org/10.1364/OL.31.001235

[17] Seyedfaraji, A., & Ahmadi, V. (2013). New design of ring-based Raman amplifier using optofluidic materials. Optical Engineering, 52(9), 097103-1 - 097103-6. https://doi.org/10.1117/1.OE.52.9.097103

[18] Seyedfaraji, A., & Ahmadi, V. (2016). Enhanced Raman amplification by conventional and hybrid photonic crystal based ring structure. Optical and Quantum Electronics, 48(190), 1-13. https://doi.org/10.1007/s11082-016-0448-7

[19] Bakhshi, S., Moravvej-Farshi, M. K., & Ebnali-Heidari, M. (2011). Proposal for enhancing the transmission efficiency of photonic crystal 60 waveguide bends by means of optofluidic infiltration. Appl. Opt., 50, 4048-4053. https://doi.org/10.1364/AO.50.004048

[20] Bakhshi, S., Moravvej-Farshi, M. K., & Ebnali-Heidari, M. (2012). Design of an ultracompact low-power all-optical modulator by means of dispersion engineered slow light regime in a photonic crystal Mach-Zehnder interferometer. Appl. Opt., 51, 2687-2692. https://doi.org/10.1364/AO.51.002687

[21] Dekker, R., Usechak, N., Först, M., & Driessen, A. (2007). Ultrafast nonlinear all-optical processes in silicon-on-insulator waveguides. J. Phys. D: Appl. Phys., 40, R249-R271. https://doi.org/10.1088/0022-3727/40/14/R01

[22] Keyvaninia, S., Ahmadi, E. D., Farman, F., Taghiabadi, R., & Bahrampour, A. (2008). Gain variation of Raman amplifier in silicon micro-ring coupled resonator optical waveguides. Proc. SPIE, 6998, 699818-1-699818-8. https://doi.org/10.1117/12.782234

[23] Kippenberg, T. J. A. (2004). Nonlinear Optics in Ultra-high-Q Whispering-Gallery Optical Microcavities (Ph.D. thesis, California Institute of Technology).

[24] Lin, Q., Painter, O. J., & Agrawal, G. P. (2007). Nonlinear optical phenomena in silicon waveguides: Modeling and applications. Optics Express, 15, 16604-16644. https://doi.org/10.1364/OE.15.016604

[25] Zheng, W., Xing, M., Ren, G., Johnson, S. G., Zhou, W., Chen, W., & Chen, L. (2009). Integration of photonic crystal polarization beam splitter and waveguide bend. Optics Express, 17, 8657-8668. https://doi.org/10.1364/OE.17.008657

[26] Xing, F. F., Borel, P. I., Frandsen, L. H., Harpøth, A., & Kristensen, M. (2004). Optimization of bandwidth in 60 photonic crystal waveguide bends. Opt. Commun., 248, 179-184. https://doi.org/10.1016/j.optcom.2004.12.003